EREM 81/2
Journal of Environmental Research, Engineering and Management
Vol. 81 / No. 2 / 2025
pp. 136–155
10.5755/j01.erem.81.2.36612

Removal of Hardness from Water and Characterization of Activated Carbon Made from Peach Pit

Received 2024/03 | Accepted after revisions 2025/01

https://doi.org/10.5755/j01.erem.81.2.36612

Removal of Hardness from Water and Characterization of Activated Carbon Made from Peach Pit

Veronica J. Gómez Zavaleta[1], Deysi M. Terrones Malca[1], Adolfo E. Guerrero Escobedo[1]*, Yrwin F. Azabache Liza[2], Ronald F. Rodriguez Espinoza[3], Juan M. Ipanaqué Roña[4]

[1] Universidad Nacional de Trujillo, Perú

[2] Universidad Nacional de San Martín, Perú

[3] Universidad Autónoma del Perú, Perú

[4] Universidad Nacional José Faustino Sánchez Carrión, Perú

***Corresponding author:** aguerreroe@unitru.edu.pe

In the present study, the influence of temperature and activating agents in the production of activated carbon from peach pits was evaluated to determine the most effective removal of water hardness. To obtain experimental data, activation was carried out using a 1:1 ratio of KOH, H_3PO_4, $ZnCl_2$, and H_2SO_4 at temperatures of 400°C, 500°C, and 600°C. The results indicate that the highest preparation yield was achieved with carbon activated by H_3PO_4 at 400°C, resulting in a 47% yield. In all activation cases, the surface acidity, determined by Boehm titration, exceeded the basic character. The predominant acidic character was obtained with $ZnCl_2$ at 500°C, reaching 62.08 mol%; acid character analyses were supported by zero-charge point pH analysis. The best iodine index analysis results were 797.22 mg/g and 747.72 mg/g, obtained with $ZnCl_2$ at 400°C and 600°C, respectively. The activated carbon with $ZnCl_2$ at 400°C demonstrated an efficiency of 66.88 % in removing water hardness, representing the highest removal compared to other activated carbons.

Keywords: activated carbon, peach pit, surface acidity, iodine index, water hardness, iodine index.

Introduction

The quality of water is a critical concern for human health and the well-being of aquatic ecosystems. Water potability implies that it does not contain objectionable contaminants such as microorganisms, chemicals, or infectious agents that could have harmful effects on people (Lin et al., 2022). To determine if water is

potable, chemical analyses are conducted to assess its electrical conductivity, density, pH, total hardness, calcium hardness, calcium, magnesium, total and partial alkalinity, and chlorides, among other parameters (Pérez-López, 2016).

Every organism requires access to potable water, although humans, in particular, depend on a purified supply enriched with minerals and salts. Water purity implies that it is free of bacteria, pathogenic microorganisms, dissolved metal ions and heavy contaminants that can have detrimental effects on health (Choparapu et al., 2020). However, climate change, severe droughts, population growth, increased demand, and mismanagement over the past decades have further strained scarce freshwater resources worldwide and have led to severe water shortages in many regions, which could become a major obstacle to public health and development (Van Vliet et al., 2021; Salehi, 2022; Tarrass and Benjelloun, 2012). Water scarcity is expected to affect socioeconomic activities, food security, education, health, and the intensity of climate change, so it has drawn public attention (Mulwa et al., 2021).

Access to basic water and sanitation services, freshwater variability, and water storage are some of the dimensions that can impact human development worldwide (Amorocho-Daza et al., 2023). In this sense, Peru is one of the countries with the lowest percentage of population with access to safe drinking water in the Latin American region (Hernández-Vásquez et al., 2021).

Water hardness, one of the undesirable attributes present in ground and surface water supplies, is a widespread problem that poses global challenges by causing mineral buildup in pipes and altering the taste of drinking water. Its origin lies in dissolved minerals, mainly calcium and magnesium compounds, present in natural sources and aggravated in municipal supplies by various factors such as saline groundwater discharge, seepage through mineral-rich soils, agricultural flows, municipal wastewater, and atmospheric deposition, which can result in negative economic consequences for households and industries (Ahn et al., 2018; Farah and Torell, 2019). Thus, the common presence of hard water in various regions of the world poses health concerns, and research in this field could address the specific needs of communities and sectors affected by water quality challenges, offering solutions that improve health and well-being in these areas (Dubey, 2022).

A study conducted in the Peruvian Andes revealed that water sources at 3500 m.a.s.l., in the dry season, present a total hardness between 77 and 355.80 mg/L, in relation to calcium carbonate, exceeding the maximum value recommended by the World Health Organization, which establishes a range between 100–300 mg/L (Choque-Quispe et al., 2021); however, the maximum permissible limit in Peruvian legislation is 500 ppm of total hardness. In the coastal zone, for example, in Lima, between 1995 and 2003, maximum total hardness values of 377 ppm for surface water and 595 ppm for groundwater have been reported. For Piura, Paita, Sullana, Chulucanas, and Talara, a maximum value of 385 ppm has been reported, while it was 1134 ppm in La Libertad and 563 ppm in Chimbote, Casma and Huarmey. In the Peruvian Amazonian rainforest, for example, Tarapoto, Lamas and Juanjuí, the maximum hardness value reported in the study was 220 ppm (SUNASS, 2004). Although in most cases the values are below the maximum limit of 500 ppm, they do not comply with the World Health Organization's recommendation.

On the health issue, there is apparently an inverse relationship between hard water intake and cardiovascular mortality, especially in case of very hard water, i.e., with hardness greater than 180 ppm, although in some studies this relationship has not been conclusive; however, consumption of water with high hardness may decrease intestinal absorption of iron, magnesium, zinc and phosphorus, triggering hypermagnesemia and subsequent renal failure (Sengupta, 2013; Morris et al., 2008; Bykowska et al., 2023).

To eliminate or reduce the presence of calcium and magnesium ions, responsible for water hardness, among various methods, previous scientific research has confirmed that activated carbon acts as highly adsorbent (Lima et al., 2020). The use of agricultural waste to obtain activated carbon represents a sustainable and environmentally friendly alternative, as it transforms this waste into a useful product for water treatment (Mo et al., 2018). Research on the production of activated carbon from peach pit could not only drive technological advances in water treatment systems and purification technologies but also generate economic benefits by offering a more efficient

and cost-effective water treatment technology, when considering the impact of temperature and activating agent in its manufacture (Moreno-Castilla, 2004; Wang et al., 2020). To produce activated carbon from agricultural waste biomass, activating agents are necessary, and the temperature must be raised to 500–1200°C (Ukanwa et al., 2019).

One of the alternatives for producing activated carbon is the reuse of agricultural waste, such as peach pits. World peach production reached 21 029 000 metric tons in the 2020/21 cycle, with China leading production (68.95%), followed by the European Union (16.52%) and Turkey (4.14%) (De Medina-Salas et al., 2022). However, a lack of control in the management of peach waste can have significant environmental impacts, including unpleasant odors, greenhouse gas emissions that contribute to global warming, and atmospheric pollution, which can have negative consequences for human health (Lam et al., 2016). In Peru, the annual peach production is approximately 35 650 t, cultivated across around 4 500 hectares, with the majority of the harvest concentrated in February and March. The peach tree, scientifically known as Prunus persica, is a deciduous fruit tree characterized by its semi-spherical fruits, which have smooth or fuzzy skin and succulent flesh (Ministerio de Comercio Exterior y Turismo del Perú, 2007). A study conducted by Takmil et al. (2020) has assessed fluoride ion adsorption using activated carbon/Fe_3O_4 nanocomposites, achieving an efficient removal of 97.4% with a surface area of 226.78 m^2/g, indicating a promising method for wastewater treatment. The study conducted by Rostami et al. (2023) focuses on the synthesis of activated carbon derived from bitter orange wood and *Amygdalus scoparia* Spach. Activation parameters, including activation time, temperature, and initial particle size, were optimized. Analytical techniques, encompassing Fourier-transform infrared spectroscopy (FT-IR) and elemental analysis, confirmed the successful surface modification, with the presence of functional groups. Furthermore, field emission scanning electron microscopy (FESEM) images revealed three-dimensional particles with an average thickness of 300–400 nm. As a complementary investigation, the study by Rostami et al. (2022) has utilized cysteine-modified activated carbon derived from orange wood for cadmium adsorption, achieving a maximum adsorption capacity of 120 mg/g under optimized conditions (pH 6, 60 min). The results demonstrated an endothermic and chemically driven process that aligned with the pseudo-second-order kinetic model (R^2 = 0.97). Javidi Alsadi and Esfandiari (2019) analyzed mercury removal from aqueous solutions using commercial activated carbon and sugarcane bagasse-derived activated carbon. The study revealed that mercury adsorption increased with higher activated carbon dosage and contact time, while decreasing with elevated mercury concentration. Notably, the bagasse-derived carbon demonstrated comparable effectiveness to commercial activated carbon in removing mercury and other heavy metals, including lead and cadmium.

Other previous studies put to test precursor materials for hardness removal. In this line, coconut shell activated carbon showed a 47% efficiency at 333 K (Rolence et al., 2014), cassava peels showed a rate of removal of 90% (Nyangi, 2023), while in the cases of *moringa oleifera*-derived seed pod husk-activated carbon resulted in a maximum removal efficiency of 59% (Varada, 2018). Other materials that have been tried are apricot shells and coconut shell powder, which have reported removal efficiencies of 80.12% and 62.58%, respectively (Al-Layla and Fadhil, 2022; Tomar, 2018).

Since water is a natural resource threatened by contamination and possible scarcity, it is imperative to treat and care for it in order to guarantee its use for future generations. Favorable results have been obtained in the removal of cationic metals from aqueous solutions through the chemical activation of carbon precursor materials, such as bitter orange wood and *Amygdalus scoparia* Spach, by varying adsorption time, activating agent, and temperature. In this context, it is important to seek alternative carbon sources for water purification and solid waste reduction through reuse or recycling. This approach will contribute to the circular economy of productive activities and environmental preservation. Therefore, the use of carbon sources such as peach pits is appropriate for activation with chemical agents to remove hardness from drinking water (Rostami et al., 2023).

This study addresses the better conditions of activated carbon synthesis from peach pits for water hardness removal, employing various activating agents (KOH, H_3PO_4, $ZnCl_2$, and H_2SO_4) and activation temperatures (400°C, 500°C, and 600°C). The research aims to develop an improved adsorbent, thus contributing to the advancement of water treatment technologies.

Furthermore, the study explores the relationship between activation parameters and the efficacy of the resulting carbon, promoting the valorization of agricultural waste products. The research question is as follows: How do temperature and activator agents influence the production of activated carbon from peach pits for reducing water hardness?

This study innovates by comprehensively optimizing the production of activated carbon from peach pits to treat water hardness. It systematically evaluates temperature and activating agents, offering a unique and detailed comparison. The discovery of optimal conditions ($ZnCl_2$ at 400°C) is significant for water treatment. The research stands out for valorizing agro-industrial waste, contributing to the circular economy and advancing water purification techniques. The novelty of this study lies in its specific focus on the adsorption of calcium and magnesium ions to treat water hardness using activated carbon from peach pits, an area that has been little explored. Unlike most research on activated carbon, this work concentrates on ionic adsorption for this particular purpose, providing valuable data on the properties and effectiveness of the material in this application. This research innovates through its detailed examination of water hardness ion adsorption using peach pit-derived activated carbon. It uniquely correlates the adsorbent's physicochemical properties with ionic adsorption capacity, providing crucial insights into adsorption mechanisms. The study addresses a significant gap in scientific literature by elucidating ionic interactions with activated carbon surfaces specifically for water softening. By focusing on the relationship between structural characteristics and adsorption efficiency, this work contributes valuable data for optimizing hard water treatment processes and adsorbent design.

Materials and Methods

Materials

The equipment and reagents used during the research included an analytical balance (Sinergy Lab, model AS R2), a Thelco Precision Scientific stove, a Barnstead Thermolyne muffle furnace (model 1600), vacuum filtration equipment with a Welch vacuum pump, a Barnstead Thermolyne magnetic stirrer (series 11511), and a JENWAY 3510 pH meter. Personal protective equipment was also employed throughout the experiments. Characterization of the activated carbon samples was performed using a Thermo Fisher Scientific scanning electron microscope (SEM) for microphotographs and electron transfer dissociation (ETD) analysis. Additionally, attenuated total reflectance (ATR) analysis was conducted with a Shimadzu IRTracer-100 FTIR spectrophotometer. Peach pit was used as the raw material for the preparation of activated carbon, while KOH (85%), H_3PO_4 (85%), and H_2SO_4 (98%), all of analytical grade, as well as $ZnCl_2$ (q.p.), served as activating agents. For the hardness removal experiments, drinking water sourced from the Physicochemical Laboratory of the National University of Trujillo, Peru, was utilized.

Methods

The methodology followed in this research is outlined below.

Activated carbon preparation

For the realization of the research, the following steps were followed: collection, washing, drying (in a cooker at 85°C during 72 hours to constant weight), grinding of the peach pit, sieving, impregnation of the sample with chemical reagent solution (KOH 40%, H_3PO_4 40%, $ZnCl_2$ 40%, H_2SO_4 40%) weight proportion 1:1, for 24 hours, neutralization, anaerobic carbonization in muffle for 60 minutes at variable temperatures (400°C, 500°C, 600°C), washing and neutralization were carried out with NaOH 1 M (Gimba et al., 2009). To prevent carbon loss due to the presence of oxygen, the covered crucible technique was used. This involves filling the crucible with the material and sealing it tightly with a lid made of the same material.

Characterization of activated carbon

The activated carbon obtained was subjected to different analyses to evaluate its physicochemical properties.

Moisture percentage

Moisture content directly influences the energy efficiency and quality of the activated carbon, affecting its porosity and adsorption capacity. To determine the moisture percentage, peach pits were chopped, and 10 g were weighed and distributed in 4 porcelain capsules. Subsequently, the samples were dried in an oven at 110°C for 3 hours. Subsequently, they were cooled in a desiccation chamber, and finally, the dry samples

were weighed (the procedure was repeated until a constant mass was achieved). This analysis was based on the ASTM D2867 – 09 Standard.

The percentage of moisture content was determined according to the equation:

$$\%H = \frac{W_i - W_f}{W_m} \times 100 \quad (1)$$

where W_i – initial weight in g; W_f – final weight in g; W_m – weight of the sample in g. For the final value, the 4 results were taken, and an arithmetic average was calculated.

Percentage of volatile

Volatile compounds in the raw material decompose and evaporate during the carbonization process, favoring the formation of pores. This analysis was based on the ASTM D5832-98 standard where the dry samples were placed inside a muffle at 500°C for 15 min, then allowed to cool in a drying hood and the calcined material was weighed and the percentage of volatile matter was calculated using the equation:

$$\%H = \frac{W_i - W_f}{W_m} \times 100 \quad (2)$$

where W_m – weight of the sample in g; $W_{nonvolatile}$ – non-volatile weight in g.

Percentage of ash

The percentage of ash in the raw material is a key indicator in the production of activated carbon, as it reflects the amount of non-combustible minerals remaining after the carbonization process. A high ash content reduces the amount of available carbon and can clog the pores of the carbon, which decreases its surface area and, consequently, its adsorption capacity. Based on the Standard to ASTM D2866-11, the samples were calcined without moisture, taking 2 g for each activated agent at a certain temperature, inside a muffle at 500°C for 3 hours, and it was left to cool in the drying hood to then quantify the weight of the ashes, making use of that weight the percentage of ashes was obtained with the equation:

$$\%C = \frac{W_f}{W_m} \times 100 \quad (3)$$

where W_f – final weight in g; W_m – weight of the sample in g.

Percentage of fixed carbon

The percentage of fixed carbon in the raw material is a fundamental parameter in the production of activated carbon since it represents the fraction of carbon that is not volatilized during the carbonization process. A high fixed carbon content is highly desirable, as it promotes the formation of a porous structure and improves the adsorptive capacity of the activated carbon. This parameter is directly related to the efficiency of the process, since a higher percentage of fixed carbon indicates a greater amount of active material available for adsorption of contaminants in various applications. To calculate the fixed carbon percentage, previously obtained values for volatile matter, ash, and moisture were used (Acevedo et al., 2017).

$$\%\text{Fixed carbon} = 100\% - (\%\text{Moisture} + \%\text{ volatiles} + \%\text{ ashes}) \quad (4)$$

Determination of point of zero charge

The point of zero charge is the pH value at which the surface of the material has no net charge, i.e., the positive and negative charges on its surface are balanced. This parameter is critical to understanding the adsorbent's behavior against different ionic species in solution because it determines whether the surface will tend to adsorb cations or anions depending on the pH of the medium. It was determined by adapting the procedure described by Newcombe et al. (1993). Activated carbon was weighed in different masses (0.10 g and 0.80 g) in amber flasks and 25 mL of 0.1 M NaCl was added to each weight; the initial pH was measured and then stirred at 25°C for 48 hours. After this time, the equilibrium or final pH was measured. The point of zero charge is obtained graphically and corresponds to the point where the final pH curve as a function of the initial pH cuts the diagonal.

Iodine index

The iodine index is a key parameter for evaluating the adsorptive capacity of activated carbon, as it measures the amount of iodine, in milligrams, that can be adsorbed by one gram of carbon. This index reflects the presence of micropores in the material, which are responsible for adsorbing small molecules, such as iodine. A high iodine index indicates a higher surface area, which translates into a higher efficiency of the

activated carbon for adsorption of contaminants. It was determined based on the international standard ASTM D4607-94: Standard test method for the determination of the iodine value of activated carbon, where 1 g of activated carbon was weighed and 10 mL of 5% HCl was added to moisten the entire sample. The sample was heated to boiling, kept there for 30 seconds and then allowed to cool to room temperature. Then 100 mL of iodine in standard solution was added to the 0.1 N stirring for 30 s. Then it was filtered, discarding the initial 20–30 mL of filtrate, and 50 mL was taken and titrated with 0.1 N sodium thiosulfate until the solution turned pale yellow. Then, 3 drops of starch were added, continuing with the titration until the solution was completely transparent.

$$\frac{X}{M} = \frac{A - 2.2 \times B \times mL\ of\ thiosulphate\ solution\ used}{g\ of\ activated\ charcoal} \quad (5)$$

where X/M: mg iodine adsorbed per g activated carbon; A = N_1 × 12 693; B = N_2 × 126.93; N_1: normality of the iodine solution, eq/L; N_2: normality of the sodium thiosulfate solution, eq/L; 2.2: factor of the aliquot when using HCl.

$$C = \frac{N_2 \times mL\ of\ spent\ thiosulphate\ solution}{25\ mL} \quad (6)$$

where C is residual normality of filtrate, eq/L.

$$IodineIndex = \frac{X}{M} \times D \quad (7)$$

where D is the normal of the corrected residual filtrate (C), correction factor.

Yield

Activated carbon yield refers to the amount of final product obtained from a given amount of raw material after the carbonization and activation processes. This parameter is essential to evaluate the efficiency of the production process, as it is influenced by factors such as raw material composition, carbonization conditions (such as temperature and time), and the removal of volatiles and ash. A high yield indicates a higher efficiency in the conversion of the raw material into activated carbon, maximizing both the amount produced and the adsorptive capacity of the final material. The yield of activated carbon obtained during the activation process was determined (Peña et al., 2012) using the following formula:

$$\%Yield = \frac{final\ dry\ mass(g)}{initial\ dry\ mass(g)} \times 100 \quad (8)$$

Percentage of burn off

The percentage burnup in activated carbon production represents the fraction of raw material that is lost during the carbonization and thermal activation processes, mainly due to the removal of volatile compounds and other impurities. Maintaining a controlled burn rate is essential to balance the removal of impurities with the preservation of activated carbon. Too high a burn-off rate can reduce the performance of the activated carbon, while too low a burn-off rate can compromise the porosity and thus the adsorptive capacity of the final product. The burn off percentage or activation yield was determined as follows (Fan et al., 2004):

$$\%burnoff = \frac{initial\ dry\ mass(g) - final\ dry\ mass(g)}{initial\ dry\ mass(g)} \times 100 \quad (9)$$

Moles of acidic and basic groups

The analysis of acidic and basic moles in an activated carbon is fundamental to characterize its surface chemistry since it allows quantifying the presence of oxygenated functional groups on its surface, which act as Brønsted-Lowry acids or bases. The proportion of these groups directly influences the activated carbon's adsorption capacity and selectivity towards certain adsorbates, affecting its effectiveness in various applications. The Boehm method was applied, as described by Broche et al. (2018). For that, 2 samples were weighed, 250 mg each, one of them was placed in a container with 50 mL of NaOH, 0.1 N, and the second one was placed in a container with 50 mL of HCl, 0.1 N. The solutions were covered and left at room temperature for 5 days. After 5 days, 10 mL samples of the solutions were taken and each one was titrated with the standard solution of NaOH and HCl as appropriate, using phenolphthalein and methyl orange as indicators. The data obtained were plotted by determining the acidic and basic groups using the following equations:

$$basic\ group\ moles = \frac{V_a(C_a) - V_{eqNaOH}(C_{NaOH})\frac{V_a}{V_{aliquot,a}}}{m} \quad (10)$$

where C_a – concentration of the acid to be reacted with the biosorbent in the mixture, eq/L; V_a – volume of the

acid that will react with the biosorbent in the mixture, mL; $V_{aliquot,\ a}$ – volume of aliquot taken, mL; C_{NaOH} – concentration of titrant, eq/L; $V_{eq\ NaOH}$ – volume of the base at which the equivalence point occurs, mL.

$$basic\ group\ moles = \frac{V_b(C_b) - V_{eqHCl}(C_{HCl})\frac{V_a}{V_{aliquot,b}}}{m} \quad (11)$$

where C_b – concentration of the base to be reacted with the biosorbent in the mixture, eq/L; V_b – volume of the base that will react with the biosorbent in the mixture, ml); $V_{aliquot,b}$ – volume of aliquot taken, ml; C_{HCl} – concentration of titrating agent, eq/L.

Activated carbon morphology

A SEM study was conducted to analyze the distribution and uniformity of micropores, mesopores, and macropores in the activated carbon. The surface morphology was examined using a Thermo Fisher Scientific electron microscope with magnifications ranging from 250x to 1000x, operating at 28.70 kV to 30 kV, and equipped with a secondary high-vacuum ETD detector. The analysis was performed at a scale of 50 µm to provide detailed insight into the pore structure.

Elemental microanalysis

The surface composition of the activated carbon, identifying and quantifying elements such as carbon, oxygen, and ash residues (metals or minerals), was carried out by elemental analysis by ETD using electron microscopy. This analysis was performed immediately after the SEM analysis in the same equipment, using the secondary ETD detector.

Attenuated total reflectance

To evaluate the chemical properties of the activated carbon surface, the functional groups present were identified, as they influence the adsorption capacity and interaction with various contaminants. A Shimadzu IRTracer100 FTIR spectrophotometer in the 400 to 4000 cm^{-1} wavenumber range was used to determine the functional groups present on the activated carbon.

Water hardness removal

A sample of drinking water was subjected to total hardness analysis prior to treatment with activated carbon. For each analysis, 25 mL of the sample was taken and mixed with 25 mL of distilled water, 10 mL of buffer solution, 3 drops of magnesium chloride $MgCl_2$ and a pinch of EBT (Eriochrome black T). They were titrated with 0.01N EDTA (Ethylenediaminetetraacetic Acid) to blue shift, and the volume spent was recorded (American Public Health Association, 2015).

$$Dt = \frac{N_{EDTA} \times V_{g,EDTA} \times 1000}{Vm} \quad (12)$$

where Dt – total hardness mg/L; N_{EDTA} – normality of EDTA solution, eq/L; $V_{g,\ EDTA}$ – volume of EDTA spent in the titration, mL; Vm – sample volume, mL.

Twelve drinking water samples were taken to which activated carbons were added, with the four activating agents at 400°C, 500°C and 600°C obtained independently and of a mesh size of less than 0.25 mm, at a ratio of 0.5 g/L. These samples were shaken at 100 rpm for 20 minutes. A 25 mL aliquot of each sample was extracted, filtering the activated carbon. Each sample was subjected to total hardness analysis. This procedure was repeated with new treatments at times of 40 and 60 minutes.

The % removal of total hardness was determined using the formula:

$$\%\ of removal of Dt = \frac{C_i - C_f}{C_i} \times 100 \quad (13)$$

where Dt – total hardness, mg/L; C_i – initial hardness of the sample, before adsorption, mg/L; C_f – final hardness of the sample, mg/L.

Research design

A randomized complete block design was used, where the blocks represent different levels of activation temperature and activating agent used. Peach pit charcoal was activated with the agents KOH, H_3PO_4, $ZnCl_2$ and H_2SO_4, each at the temperatures of 400°C, 500°C and 600°C. Each activated carbon sample was characterized, and finally these samples were used to remove hardness from the drinking water of the laboratory.

The tests were conducted considering two variables: activating agents and temperature, with 4 and 3 levels, respectively. A total of 12 experiments were performed, with 3 analyses conducted for each experiment, resulting in 36 experimental data points. *Table 1* shows the experimental design of the research. The results coded with "ab" are the average values of hardness removal.

Table 1. *Experimental design of the research*

Activating agent	Temperature (°C)		
	400 (b1)	500 (b2)	600 (b3)
KOH (a1)	a1b1	a1b2	a1b3
H_3PO_4 (a2)	a2b1	a2b2	a2b3
$ZnCl_2$ (a3)	a3b1	a3b2	a3b3
H_2SO_4 (a4)	a4b1	a4b2	a4b3

Statistical analysis

To evaluate the significance of the variables on the hardness removal percentage, Minitab v.19 software was used. For the analysis of variance, the General Linear Regression Model was applied, configuring the response variable as the hardness removal percentage, the factor as the type of activating agent, and the covariates as temperature, time, iodine index, and percentage of acidic moles. The iodine index variable was nestled with the type of activating agent.

Results and Discussion

Characterization of raw material and activated carbon performance

The moisture and ash content in the raw material are key parameters in the production of activated carbon, as they directly affect process efficiency and product quality. High moisture content increases energy costs due to the need to remove water during carbonization, while a high ash percentage reduces the amount of available active carbon, negatively impacting adsorption capacity.

Preliminary analyses of peach pit, presented in *Table 2*, reveal a low moisture content (8.25%) and a reduced percentage of ash (0.8%), results very close with those reported in previous studies (Uysal et al., 2014; Calixtro, 2016; Filippín et al., 2017).

Table 2. *Preliminary analysis of peach kernel*

Essay	Result
% Humidity	8.25
% volatile matter	77.15
% ashes	0.80
% fixed carbon	13.8

Fig. 1 shows the percentage yield obtained with the activating agents used at temperatures of 400°C, 500°C and 600°C.

The chemicals H_3PO_4, $ZnCl_2$, and H_2SO_4 showed higher yields at all temperatures compared to KOH, with the best value of 47% for the activated carbon treated with H_3PO_4. The lowest yield was 24.3% for activated carbon with KOH at 600°C, similar to that obtained for physically activated carbons with the same raw material (Reyna and Chuquilín, 2006) or chemically activated with $ZnCl_2$, with yields between 28% and 41% (Uysal et al., 2014). Generally, at higher temperatures, the yield decreases due to carbon loss through oxidation or release of volatile materials.

Fig. 1. *Performance of activated carbon production*

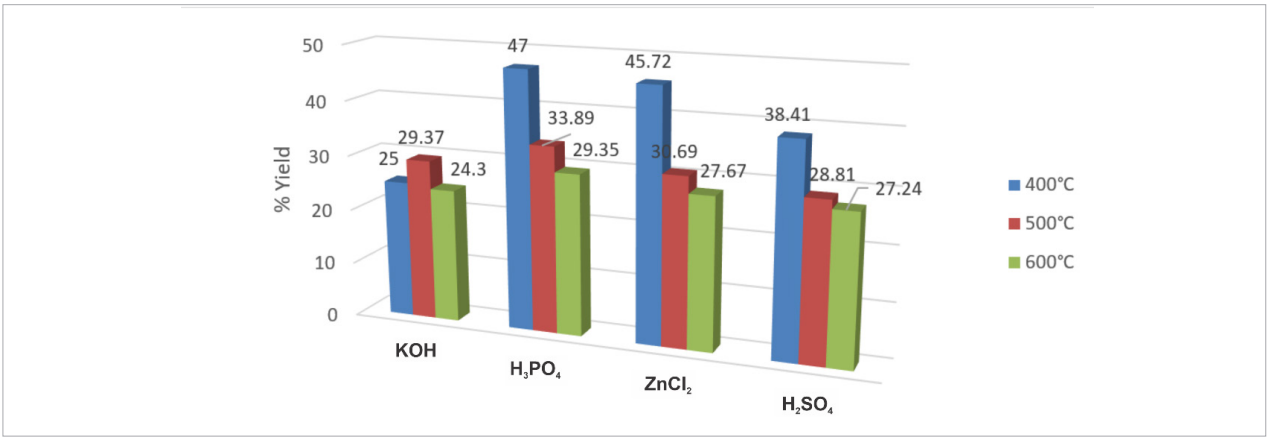

From the results in *Fig. 1*, it is inferred that in the KOH-activated carbon, there is excessive loss of carbonaceous material due to vigorous reactions with carbon at relatively low temperatures, which can lead to overactivation. The precursor material used is prone to degradation during the activation process. The elemental analysis (EDT) in *Fig. 7* provides a clear view of the potential formation of oxidation substances or elements as a result of interaction with KOH, such as CO, CO_2, H_2O, H_2, K, K_2O, and K_2CO_3 (Otowa et al., 1993).

The carbon activated with KOH presents the lowest yields due to the collapse of its carbon structure, since short activation times (6 hours) do not favor porosity and long activation times (24 hours) cause the collapse of the carbon structure. There have been reported works with KOH, $ZnCl_2$ and H_3PO_4 where it is corroborated that lower yields are obtained with KOH, although smaller pore sizes; however, for the present investigation, the burn off percentages obtained with KOH, shown in *Fig. 3*, are the highest, revealing that they were closer to pores of the macropore type (Iwanow et al., 2020). Yields of the activated carbons with KOH decrease while increasing the temperature as well as the impregnation ratio (Bag et al., 2020).

Characterization of activated carbon

The determination of the iodine index revealed that the activated carbon prepared with $ZnCl_2$ at 400°C exhibited the highest adsorption capacity, with a value of 797.22 mg/g, followed by the carbon activated with $ZnCl_2$ at 600°C, which showed an iodine index of 747.72 mg/g. These findings, as shown in *Fig. 2*, underscore the effectiveness of $ZnCl_2$ as an activating agent, particularly at lower temperatures, in enhancing the adsorption properties of the carbon.

As the iodine index is around 700 mg/g, it can be considered that the activated carbons obtained have potential to be commercialized since the specific areas are high, thus generating an improvement in the adsorption phenomenon (Asimbaya et al., 2015). The iodine value results reveal the clear superiority of $ZnCl_2$ as an activating agent compared to KOH, H_3PO_4 and H_2SO_4. Activated carbon with $ZnCl_2$ at 400°C exhibits the highest iodine value (792.2 mg/g), significantly outperforming the other agents at all activation temperatures evaluated. The superior efficacy of $ZnCl_2$ in terms of iodine value can be explained by several factors: first, its ability to promote a more controlled dehydration and degradation of the carbonaceous precursor, resulting in an optimal distribution of micropores and mesopores that are ideal for iodine adsorption; second, $ZnCl_2$ likely creates a more favorable surface chemistry with functional groups that increase the affinity for iodine molecules. In addition, its less corrosive nature compared to H_3PO_4 and H_2SO_4 allows for better preservation of the carbon structure during activation, while its higher reactivity compared to KOH facilitates the creation of a more developed porosity. The activation temperature of 400°C appears to be optimal for $ZnCl_2$, providing an ideal balance between porosity development and preservation of the carbonaceous structure, factors that are compromised at higher temperatures, as evidenced by the decrease in the iodine value at 600°C.

Fig. 2. *Iodine index at different temperatures and activating agents*

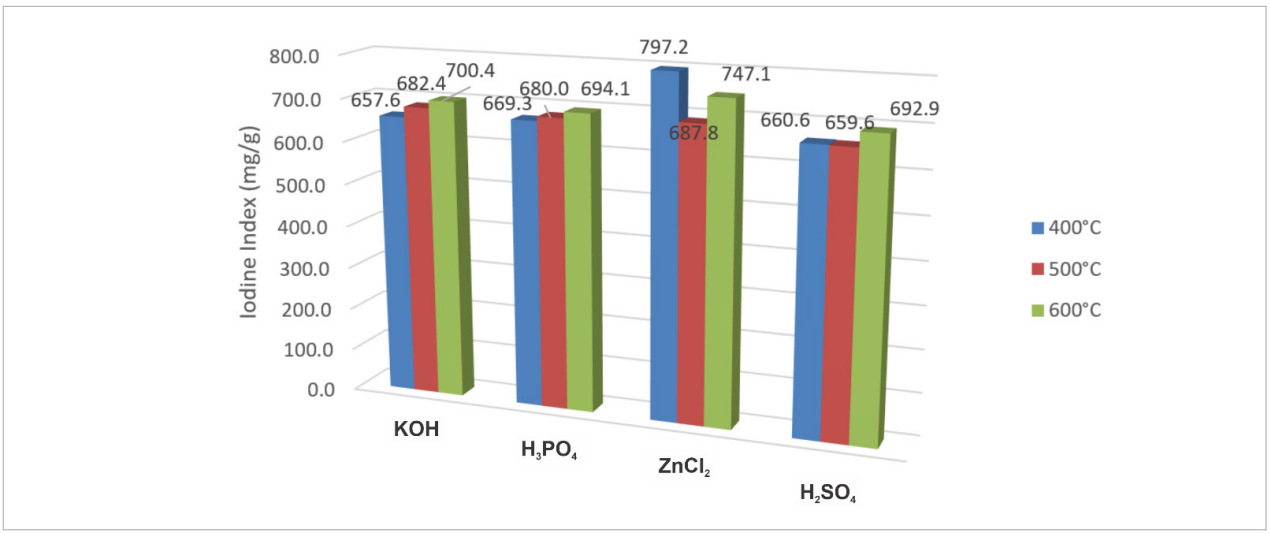

Although the best results in terms of iodine index were obtained with $ZnCl_2$, for other raw materials the effects of the activating agents may vary, being able to give better results with any of the other three agents used in this research. This suggests that the raw material's initial characteristics are predominant in the activity of the chemical substances responsible for modifying its carbonaceous structure (Adibfar et al., 2014; Girgis et al., 2002; Guo and Lua, 1999).

The obtained burn off results, according to *Fig. 3*, vary from a minimum of 53% with the H_3PO_4 activant at 400°C to a maximum of 75.7 % with the KOH activant at 600°C.

Mohd et al. (2015) state that at burn-off percentages between 50% and 75%, a combination of micropores and macropores is formed. Therefore, the activated carbons used in this research contain a mixture of both types of pores.

Fig. 4 shows that the minimum value of the point of zero charge is for $ZnCl_2$ at 400°C at pH 4.33 and the maximum value is given for $ZnCl_2$ at 600°C at pH 7.

Fig. 3. *Percentage of burn off at different temperatures and activating agents*

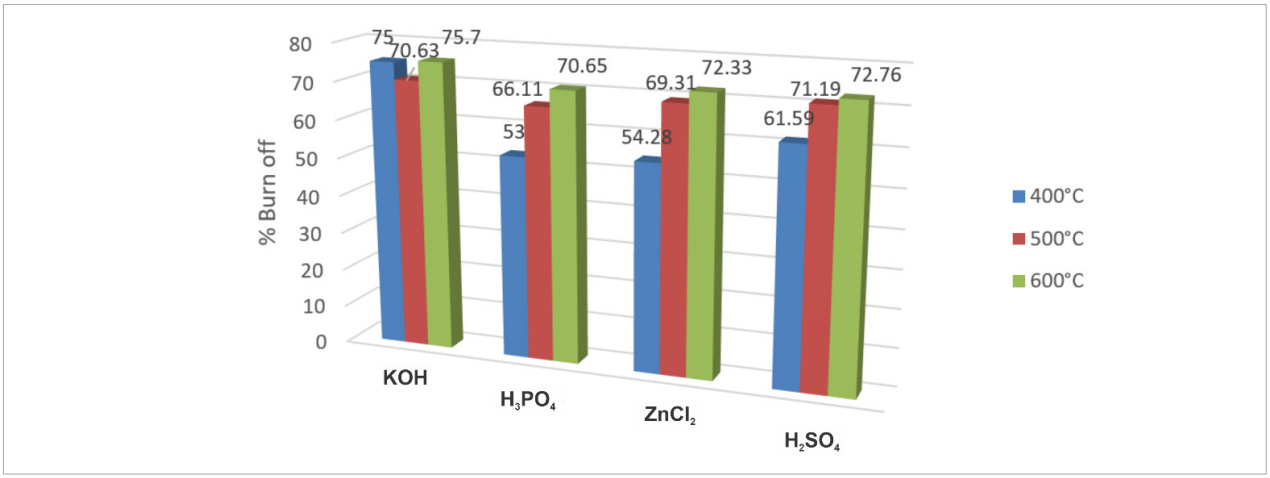

Fig. 4. *Point of zero charge at different temperatures and activating agents*

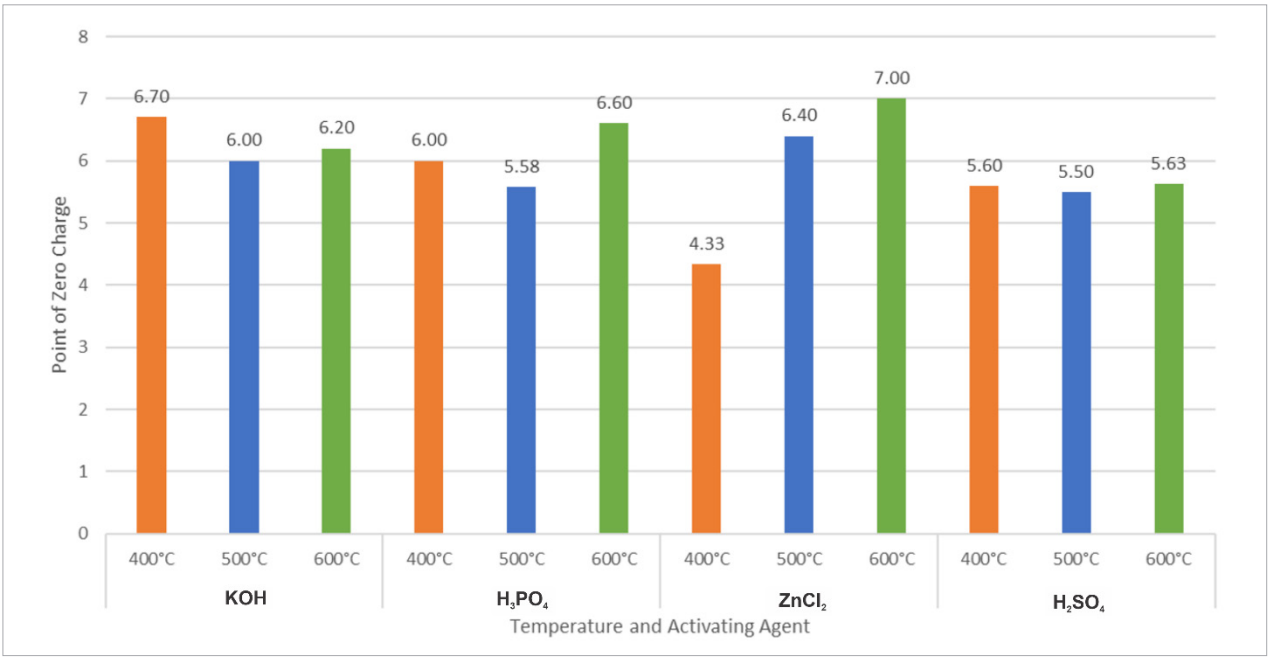

Fig. 5. *Mol percentage of acid and basic groups at different temperatures and activating agents*

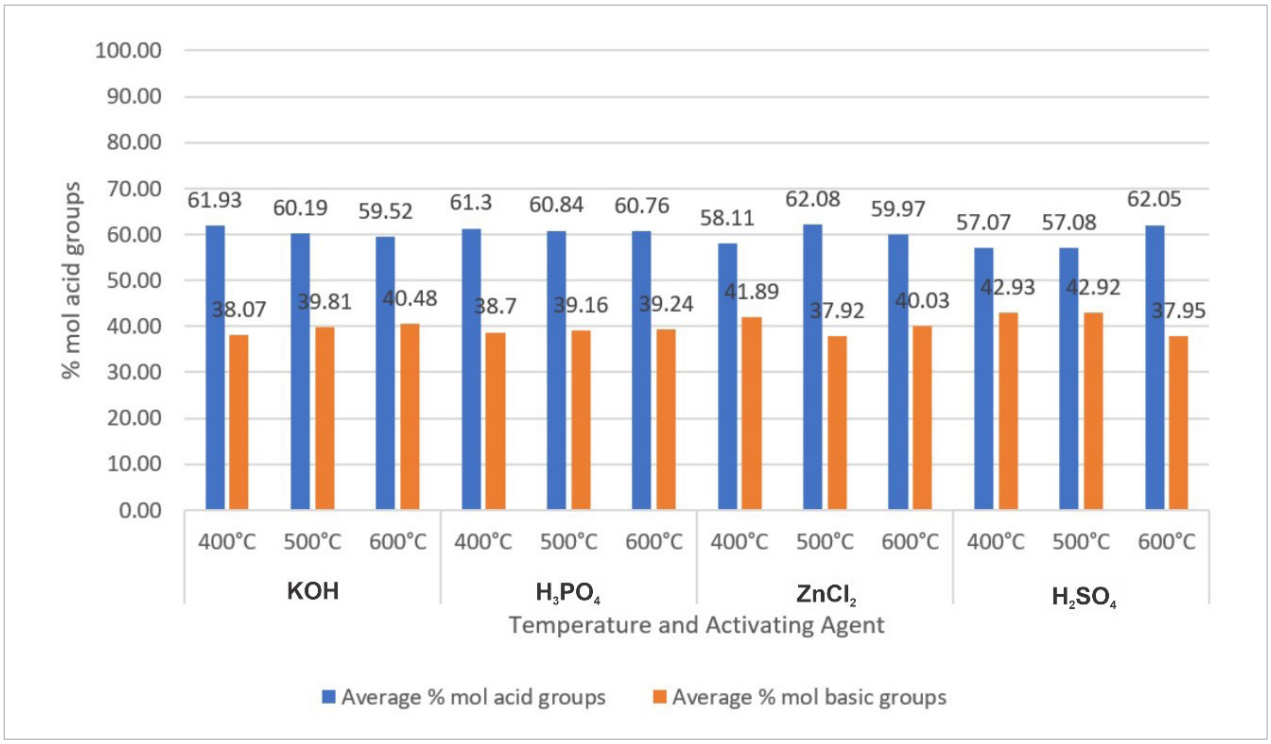

Thus, for $ZnCl_2$ at 400°C, pH values higher than 4.33 will generate a negatively charged surface, while lower values will generate a positively charged surface, and the same analysis corresponds for the rest of the activants at the other temperatures evaluated. It is then explained, evaluating the same case, that at pH higher than 4.33 the cations present in the water to be treated will be attracted, including those that generate total hardness (calcium and magnesium ions). The point of zero charge is quite useful to explain the interactions between the adsorbent and adsorbate due to charges (Amaringo Villa, 2013; Rostamian et al., 2014).

The results shown in *Fig. 5* indicate that the surfaces of all samples are conformed by a higher amount of acid groups in a range of 57.07 mol%, corresponding to the activated carbon with sulfuric acid at 400°C, up to 62.08 mol% belonging to the activated carbon using $ZnCl_2$ at 500°C.

In *Fig. 6* and *Table 3*, oxygenated functional groups are identified. *Fig. 7* reports the EDT elemental analyses where the presence of oxygen is corroborated in most of the SEM photographs. The increase in acidity is due to the presence of oxygenated groups on the carbon surface and to the decrease of the π electron density at the edges of the graphene layer, while an increase in basicity is due to regions rich in π electrons delocalized in basal planes (Vanegas, 2021). The chemical composition of activated carbons plays a crucial role in determining their adsorption capabilities, as well as their surface area and porosity. The oxygen-containing functional groups are key characteristics, as they define the surface properties of the carbons and, consequently, their effectiveness as adsorbents (Uysal et al., 2014).

In this research, the presence of oxygenated functional groups was identified, as shown in *Fig. 6* and *Table 3*. Additionally, *Fig. 7* presents elemental analysis (EDX), confirming the presence of oxygen across most of the SEM images. The increased acidity of the activated carbons can be attributed to these oxygenated groups on the carbon surface, as well as the reduction in the π-electron density at the edges of the graphene layers. In contrast, the increase in basicity is linked to π-electron-rich regions in the basal planes. These findings suggest that the chemical composition of the activated carbons, particularly the oxygenated functional groups, plays a pivotal role in determining their adsorption capacities, surface area, and porosity. The presence of these oxygen-containing groups is a critical factor

Fig. 6. *Attenuated total reflectance (ATR) of the activated carbon samples at 400°C, 500°C and 600°C temperatures*

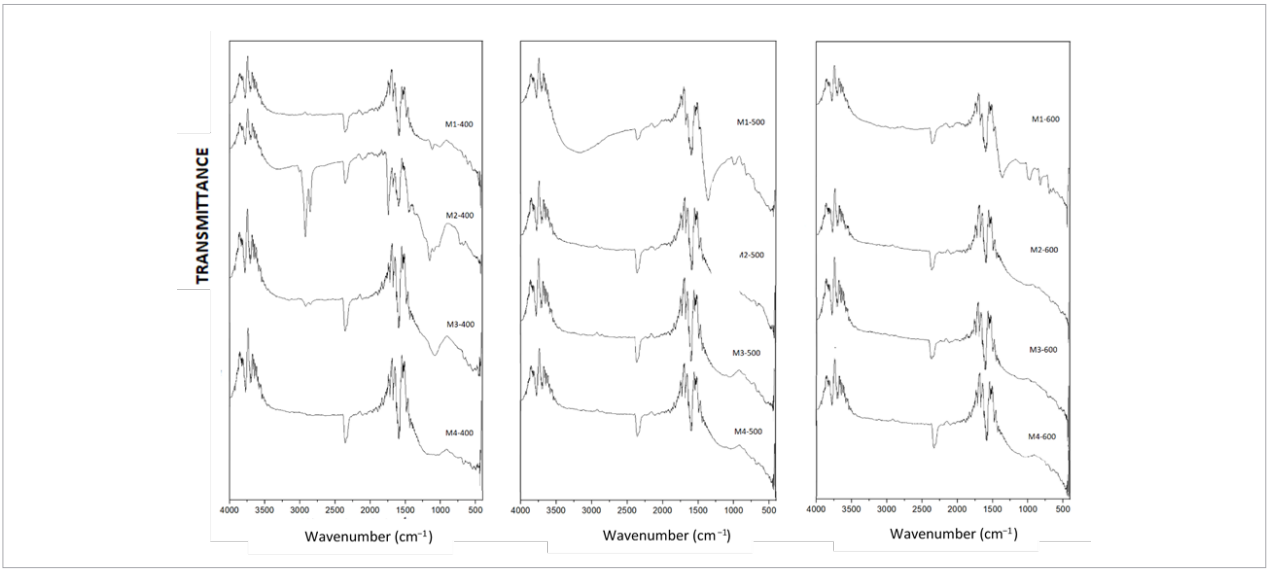

in defining the surface properties of the carbons and, consequently, their effectiveness as adsorbents. This is further supported by the literature, where similar behavior has been noted (Vanegas, 2021; Uysal et al., 2014). However, our results clearly emphasize the direct influence of these functional groups on the adsorption efficiency of the activated carbons evaluated in this study, advancing the understanding of their role in surface chemistry.

Fig. 6 shows the peaks at certain transmittances and wavenumbers according to ATR analysis of the samples. It shows defined zones to interpret in the range of 3500–4000 cm^{-1}, peaks with little definition between 2800 cm^{-1} and 3000 cm^{-1}, another zone between 2300 cm^{-1} and 1200 cm^{-1}, and the fingerprint zone between 600 cm^{-1} and 1200 cm^{-1}. Exceptionally, the signal is seen between 3270 cm^{-1} and 3300 cm^{-1} for the carbons activated with the agents KOH at 500°C and H_3PO_4 at 400°C.

Detailed wave numbers, identification of functional groups, and their interpretation are shown in *Table 3*. In addition, references to investigations with activated carbon where the same functional groups have been found have been placed.

SEM microphotographs and ETD analysis of the activated carbon samples reveal a scale of 50 µm in nearly all images, with some showing the presence of crystals, likely due to the formation of oxides from elements in the activating compounds. The detection of oxygen indicates the presence of oxygenated functional groups, confirming the identification made through ATR analysis. As shown in *Fig. 7*, oxygen is present in all samples except for those depicted in *Figs. 7c* and *7i*.

Figs. 7a, 7b, and *7c* confirm the presence of carbon, oxygen, and potassium. The production of microporosity with KOH is associated with its high reactivity. This process results in reduced performance due to the loss of carbon as CO and CO_2, consistent with previous findings (Doğan et al., 2020). In *Fig. 7d*, only carbon and oxygen are detected, whereas in *7e* and *7f*, phosphorus is also observed. Phosphoric acid (H_3PO_4) interacts with carbon to produce P_4, P_4O_{10}, CO, and H_2O, contributing to a higher yield compared to KOH, as carbon is released as CO gas (Khalil et al., 2021; Neolaka et al., 2023). In *Fig. 7h*, zinc (Zn) is identified, and in *7i*, chlorine (Cl) is detected. Although the activation mechanism of $ZnCl_2$ is not fully understood, the significantly smaller ionic radius of the Zn^{2+} cation (74 pm) compared to Na^+ (102 pm), K^+ (138 pm), and Ca^{2+} (100 pm) likely contributes to the formation of mesopores (> 2 nm), as also noted in the literature (Bergna et al., 2022; Xing et al., 2023). *Figs. 7j* and *7k* show the presence of oxygen resulting from oxidation by H_2SO_4. In contrast, *Fig. 7l* shows no oxygen, although H_2SO_4 introduces carbonyl and phenolic groups on the carbon surface. EDT revealed no sulfur (S) at activation temperatures of 400°C, 500°C, and 600°C, which is consistent with the boiling and melting points of sulfur (444.6°C and 119°C, respectively). However,

Table 3. *Identification and interpretation of functional groups in activated carbon*

Wave number	Identification	Interpretation	Reference
3792.0 cm^{-1} for all carbons	C-H	Present in alkenes, alkynes.	Bohórquez et al. (2008)
3687.5 cm^{-1} for all carbons	O-H	Present in carboxylic acids or phenols.	Bohórquez et al. (2008)
3625.0 cm^{-1} for all carbons	C = O	Present in aldehydes or ketones.	Bohórquez et al. (2008)
3580.0 cm^{-1} for all carbons	O-H	Present in alcohols or phenols. The hydroxyl groups correspond to the elongation vibration of the O-H functional group, which can be related to another peak located at 680 cm^{-1} which corresponds to the bending of the C-C bond of the Aryl-O-H functional group.	Bohórquez et al. (2008)
3270 cm^{-1} for KOH at 500°C and 3300 cm^{-1} H_3PO_4 at 400°C	O-H	Presence of moisture in those samples, which is common as appreciated in other investigations.	Rostamian et al. (2014), Doğan et al. (2020), Fortunato et al. (2022), Xing et al. (2023)
2900 cm^{-1}, 2800 cm^{-1} for H_3PO_4 at 400°C	C-H	Saturated aliphatic.	Mopoung et al. (2018) and Mojoudi et al. (2019)
2300 cm^{-1} for all carbons	CO_2 and CO presence	Functional groups are transformed into volatile CO_2 and CO and are expelled from the structure as a result of pyrolysis at high temperature; however, it may be due to sample contamination.	Chen et al. (2003) and Fortunato et al. (2022)
2125 cm^{-1} for all carbons	C≡N	Nitrile groups or cyanides.	Figueiredo et al. (1999)
2042 cm^{-1} for all carbons	C=O	Present in esters or anhydrides.	Uysal et al. (2014)
1750 cm^{-1} for all carbons	C=O	Present in aldehydes, ketones, carboxylic acids or anhydrides.	Uysal et al. (2014)
1580 cm^{-1} for all carbons	C=C-C=C	Conjugated alkenes or aromatic rings.	Khalil (2021)
1490 cm^{-1} for all carbons	C=C-C=C	Conjugated alkenes or substituted aromatic rings.	Mojoudi et al. (2019)
1450 cm^{-1} for all carbons	C-H	Assigned to asymmetric and symmetric C-H bending vibrations.	Mojoudi et al. (2019)
Moderate intensity peaks between 1400 cm^{-1} and 1700 cm^{-1}	C=O and C=C	It can be attributed to elongations. May indicate the presence of ketones, esters, aldehydes and carboxylic acids.	Shin et al. (1997)
1350 cm^{-1} for KOH-activated carbon at 500°C and 600°C	C=O	Corresponding to the acyl functional group of the esters, lactones.	Duranoğlu et al. (2010)
1350 cm^{-1} for KOH-activated carbon at 400°C	C=O	The peak is very weak.	Duranoğlu et al. (2010)
1125 cm^{-1} for all carbons	C-O	Corresponding to ethers or alcohols, stretching vibrations (phenol, COO^-).	Arriagada et al. (1997)
680 cm^{-1} for all carbons	C-H	Alkenes, alkynes or aromatic rings.	Tsoncheva et al. (2018)
1200 cm^{-1} and 980 cm^{-1} at 400°C and 500°C, for the H_3PO_4 activated carbons	P=O	Weak signals, P=O hydrogen bond stretching mode and the ionized P^+-O^- bond in the acid phosphate esters or symmetric vibrations in the P-O-P (polyphosphate) chain respectively; however, at 600°C, they were not detected.	Ali et al. (2020)
529 cm^{-1} for the three $ZnCl_2$ activated samples	Zn-O	A weak signal corresponding to the vibration of the Zn-O bond.	Tsoncheva et al. (2018), Zhao et al. (2022)

Fig. 7. *SEM microphotography and ETD analysis of activated carbon samples*

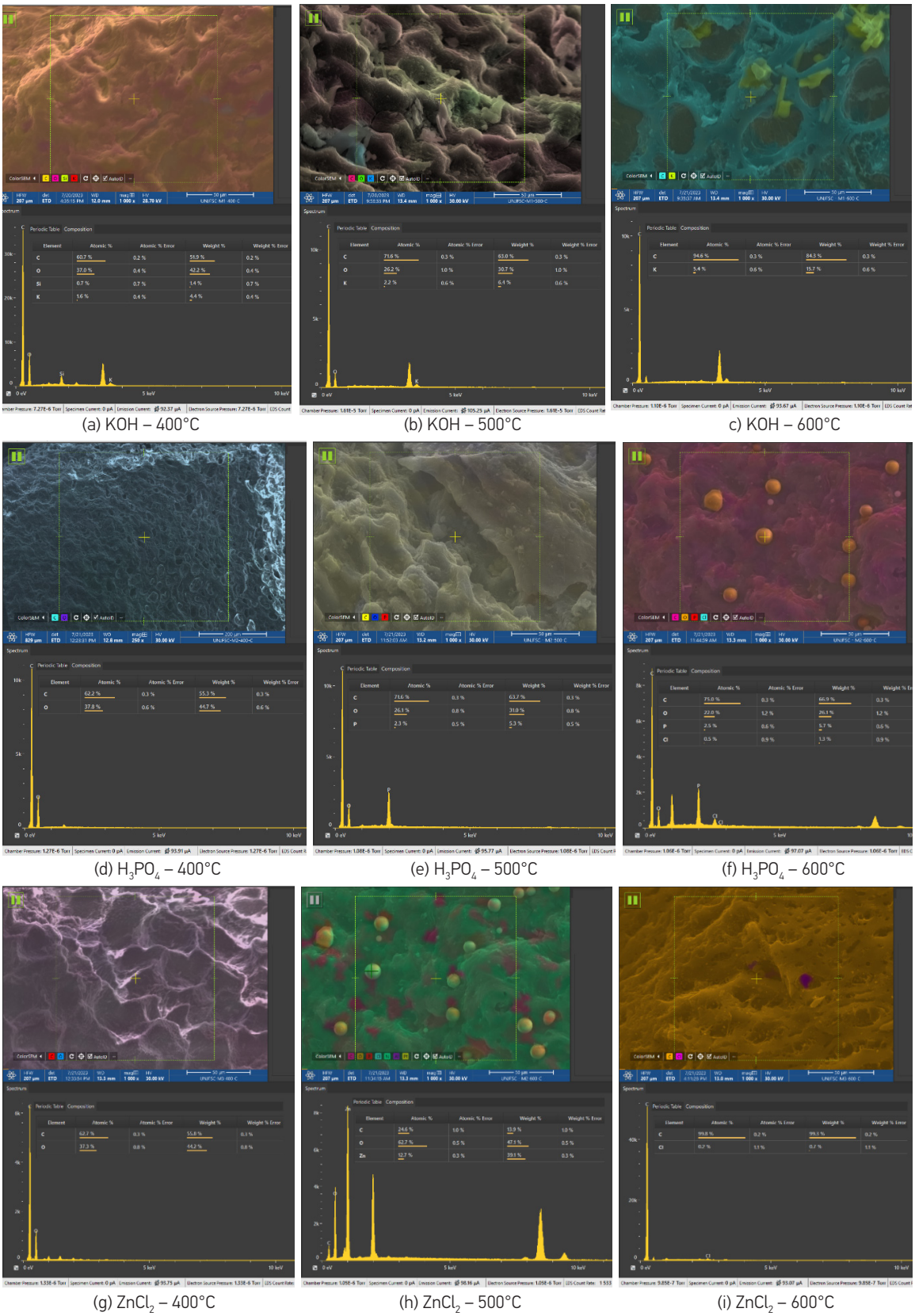

(a) KOH – 400°C (b) KOH – 500°C c) KOH – 600°C

(d) H_3PO_4 – 400°C (e) H_3PO_4 – 500°C (f) H_3PO_4 – 600°C

(g) $ZnCl_2$ – 400°C (h) $ZnCl_2$ – 500°C (i) $ZnCl_2$ – 600°C

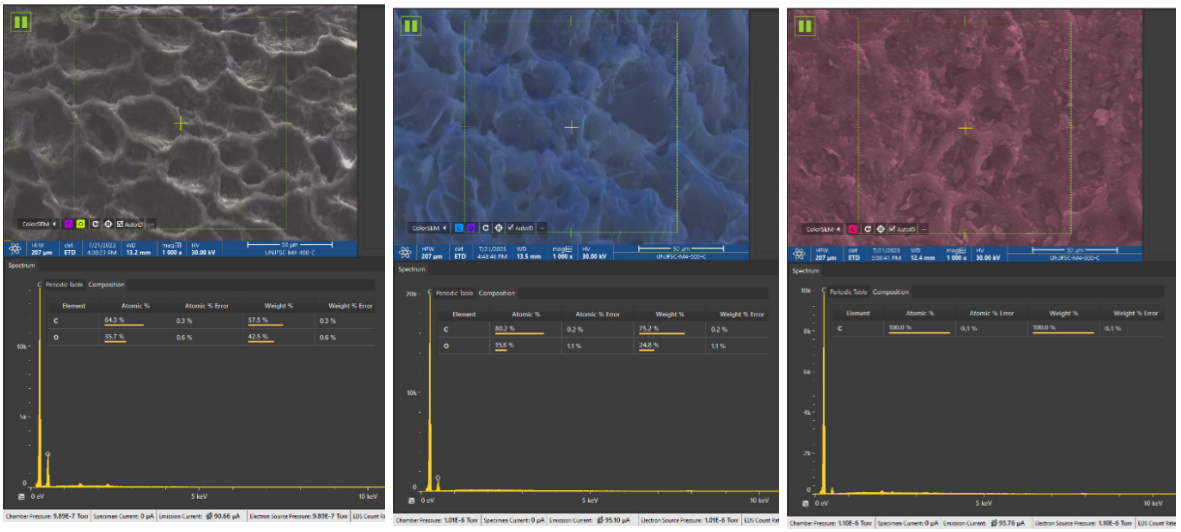

(j) H_2SO_4 – 400°C (k) H_2SO_4 – 500°C (l) H_2SO_4 – 600°C

at lower activation temperatures (108°C to 110°C), the presence of sulfur has been observed in EDX and FTIR analyses, supporting previous studies (Dao and Le Luu, 2020; Meshram et al., 2022).

Water hardness removal

The different hardness removal percentages at activation temperatures of 400°C, 500°C, and 600°C, as well as adsorption times of 20, 40, and 60 minutes for each chemical activating agent, are presented in *Fig. 8a*. The lowest removal percentages were observed with KOH at 600°C, H_2SO_4 at 500°C, and H_2SO_4 at 400°C. *Fig. 8 b* shows that the best removals were obtained at 60 minutes with the activating agents $ZnCl_2$ at 600°C, H_3PO_4 at 500°C and $ZnCl_2$ at 400°C.

The hardness removal percentages were plotted in *Fig. 8a* at the corresponding temperatures. The highest hardness removal percentages are achieved at a 60-min adsorption time with $ZnCl_2$, H_3PO_4 and again with $ZnCl_2$ at the temperatures of 400°C, 500°C and 600°C, respectively. For a 20-min adsorption time, it is observed that at 600°C for the activating agents KOH, H_3PO_4, $ZnCl_2$ the lowest percentages of removals are obtained. *Fig. 8b* compares the carbons with the best hardness removal

Fig. 8. *Hardness removal from activated carbon with activating agents at different temperatures and adsorption times*

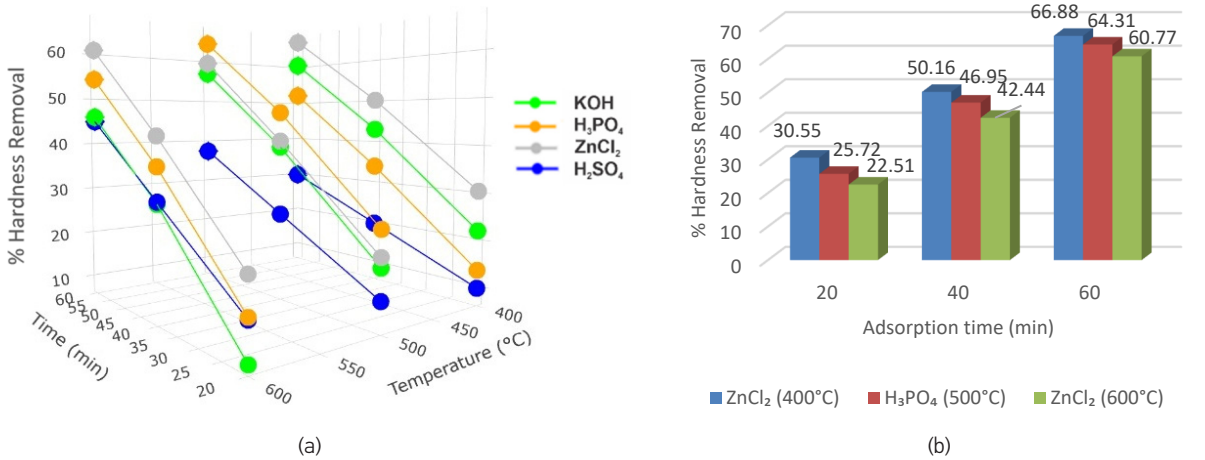

(a) (b)

percentage results. It is observed that a higher percentage of hardness removal is achieved with the activated carbon with $ZnCl_2$ at 400°C, managing to remove hardness up to 66.88% in 60 minutes. This maximum removal is explained by the better physicochemical properties of the carbon obtained with this activating agent, such as the iodine index, mixture of micropores and macropores, as well as the acidic character; a pH above 4.33 will ensure a negatively charged surface, by deprotonation of the functional groups that are present, favoring the migration of cations present in the water to the carbon surface.

The results of this investigation indicate that while iodine index generally increases with temperature (as shown in *Fig. 2*), the hardness adsorption capacity does not follow the same trend, particularly in the case of $ZnCl_2$ at 400°C (Li et al., 2002; Mojoudi et al., 2019). Our findings demonstrate that the increase in activation temperature often leads to the formation of larger pores due to reactions between the activating agent and carbon, which enhances iodine adsorption. However, the adsorption of hardness-related ions, such as Ca^{2+} and Mg^{2+}, is more complex and does not necessarily correlate with higher iodine values or larger pore sizes. The ionic radii of Ca^{2+} (0.106 nm) and Mg^{2+} (0.081 nm) suggest that these ions are more likely to be adsorbed in micropores smaller than 2 nm, but mesopores and macropores also play a crucial role in facilitating ion transport and overall adsorption capacity. This observation is consistent with our results, which show a burn-off percentage between 50% and 75%, indicating the presence of both micropores and macropores in the activated carbons studied. The pore structure, with a substantial fraction of micropores, plays a critical role in the adsorption of these ions, supporting the idea that pore size distribution is a key factor in optimizing adsorption capacity (Snyder et al., 1990). These findings emphasize the importance of pore size, shape, and distribution in optimizing adsorption for specific contaminants, independent of general trends in iodine adsorption (Gregg et al., 1967).

Statistics

The results of the general linear model for hardness removal reveal that multiple factors significantly influence the process (*Table 4*). The analysis of variance shows that all independent variables: temperature, time, acid mol, activant, and iodine index (activant) are statistically significant ($P < 0.05$). Among them, time stands out as the most influential factor, with the highest F value (379.76), followed by acid mol (7.65) and iodine index (activant) (6.48). Although temperature is significant, it has the lowest relative impact (F = 6.20).

Table 4. *Analysis of variance of the effects of the variables on the percentage of hardness removal*

Item	F Value	*P* Value
Temperature	6.20	0.020
Time	379.76	0.000
mol acid	7.65	0.011
Activant	5.14	0.007
Iodo index (Activant)	6.48	0.001

According to *Table 5*, the model presents a good fit, with an R^2 of 94.51% and an adjusted R^2 of 92.32%, indicating that it explains a large proportion of the variability in hardness removal. The robustness of the model is reflected in its high predictive power (R-squared pred = 89.34%), suggesting its potential applicability under similar conditions. The significance of the 'Activant' factor and its interaction with the iodine index underlines the importance of proper selection of the activating agent in the process. The four levels of the activant (H_2SO_4, H_3PO_4, KOH, $ZnCl_2$) show differential effects, which could have significant implications for the optimization of the hardness removal process.

Table 5. *Summary of statistical modeling for the linear regression of hardness removal percentage*

Standard deviation	R-squared	R-squared (adjusted)	R-squared (predicted)
5.2255	94.51%	92.32%	89.34%

Conclusions

The maximum removal of hardness from drinking water was 66.88% and was obtained with $ZnCl_2$ activated carbon at 400°C during a treatment time of 60 minutes. With this agent at 400°C, the highest iodine index of 797.2 mg/g was obtained indicating a greater surface area compared to the other agents used, and the burn-off percentage of 54.28% indicates that the carbon contains a mixture of micropores and macropores. This

coal is acidic in nature with an acidic group content of 58.11 mol%; likewise, the pH at zero loading point was 4.33. The ATR analyses revealed that the activated carbons exhibited carbon–carbon double bonds, hydroxyl (–OH) groups, carbon–oxygen bonds, and elements originating from the activating agents, such as phosphorus (P), zinc (Zn), and sulfur (S), which were detected in the fingerprint region of the spectra.

References

Acevedo S., Giraldo L. and Moreno J. (2017) Caracterización de carbones activados modificados con agentes quelantes para la adsorción de metales tóxicos en solución acuosa [Characterization of chelating agent-modified activated carbons for the adsorption of toxic metals in aqueous solution]. Afinidad. Journal of Chemical Engineering Theoretical and Applied Chemistry 74(578). Available at: https://raco.cat/index.php/afinidad/article/view/326510 (accessed 5 May 2024) (in Spanish).

Adibfar M., Kaghazchi T., Asasian N. and Soleimani M. (2014) Conversion of poly(ethylene terephthalate) waste into activated carbon: chemical activation and characterization. Chemical Engineering and Technology 37(6): 979–986.

Available at: https://doi.org/10.1002/ceat.201200719

Ahn M., Chilakala R., Han C. and Thenepalli T. (2018) Removal of hardness from water samples by a carbonation process with a closed pressure reactor. Water 10(1): 54. Available at: https://doi.org/10.3390/w10010054

Ali R., Aslam Z., Shawabkeh R., Asghar A. and Hussein I. (2020) BET, FTIR, and RAMAN characterizations of activated carbon from waste oil fly ash. Turkish Journal of Chemistry 44(2): 279–295. Available at: https://doi.org/10.3906/kim-1909-20

Al-Layla A. and Fadhil A. (2022) Removal of calcium over apricot shell derived activated carbon: kinetic and thermodynamic study. Chemical Methodologies 6: 10-23.

Amaringo F. (2013) Determinación del punto de carga cero y punto isoeléctrico de dos residuos agrícolas y su aplicación en la remoción de colorantes [Determination of the point of zero charge and isoelectric point of two agricultural residues and their application in dye removal]. Revista de Investigación Agraria y Ambiental 4(2): 27. Available at: https://doi.org/10.22490/21456453.982 (in Spanish).

American Public Health Association (2015) Standard methods for the examination of water and wastewater. Baird R. and Eaton A. E. (eds.). 23rd Ed.

Amorocho-Daza H., van der Zaag P. and Sušnik J. (2023) Access to water-related services strongly modulates human development. Earth's Future 11(4). Available at: https://doi.org/10.1029/2022EF003364

Arriagada R., García R., Molina-Sabio M. and Rodriguez-Reinoso F. (1997) Effect of steam activation on the porosity and chemical nature of activated carbons from Eucalyptus globulus and peach stones. Microporous Materials 8(3–4): 123–130. Available at: https://doi.org/10.1016/S0927-6513(96)00078-8

Asimbaya C., Rosas N., Endara D. and Guerrero V. H. (2015) [Obtaining activated carbon from lignocellulosic residues of canelo, laurel, and eucalyptus]. Revista Politécnica 36(3): 24–24. Available at: https://revistapolitecnica.epn.edu.ec/ojs2/index.php/revista_politecnica2/article/view/537 (accessed 5 April 2024) (in Spanish).

Bag O., Tekin K. and Karagoz S. (2020) Microporous activated carbons from lignocellulosic biomass by KOH activation. Fullerenes, Nanotubes and Carbon Nanostructures 28(12): 1030–1037. Available at: https://doi.org/10.1080/1536383X.2020.1794850

Bergna D., Varila T., Romar H. and Lassi U. (2022) Activated carbon from hydrolysis lignin: effect of activation method on carbon properties. Biomass and Bioenergy 159: 106387. Available at: https://doi.org/10.1016/j.biombioe.2022.106387

Bohórquez N., Giraldo L. and Moreno-Pirajáan J. C. (2008) Entalpías de Inmersión de Carbones Activados en Soluciones Séricas de Carbamazepina [Immersion enthalpies of activated carbon in carbamazepine serum solutions]. Información Tecnológica 19(1). Available at: https://doi.org/10.4067/S0718-07642008000100013 (in Spanish).

Broche M., Rodríguez I., Coca Y. and Calero de Hoces M. (2018) Caracterización de los residuos agrícolas de sorgo para su uso como material biosorbente de colorantes [Characterization of sorghum agricultural residues for their use as biosorbent material for dyes]. Centro Azúcar 45(4): 64–75. Available at: https://biblat.unam.mx/es/revista/centro-azucar/articulo/caracterizacion-de-los-residuos-agricolas-de-sorgo-para-su-uso-como-material-biosorbente-de-colorantes (accessed 7 May 2024) (in Spanish).

Bykowska-Derda A., Spychala M., Czlapka-Matyasik M., Sojka M., Bykowski J. and Ptak M. (2023) The relationship between mortality from cardiovascular diseases and total drinking water hardness: systematic review with meta-analysis. Foods 12(17): 3255. Available at: https://doi.org/10.3390/foods12173255

Calixtro L. (2016) Aprovechamiento del Endocarpio de la Pepa de durazno para producir carbón activado [Utilization of peach seed endocarp to produce activated carbon]. Universidad César Vallejo. Available at: https://hdl.handle.net/20.500.12692/821 (accessed 5 May 2024) (in Spanish).

Chen X., Farber M., Gao Y., Kulaots I., Suuberg E. M. and Hurt R. H. (2003) Mechanisms of surfactant adsorption on non-polar, air-oxidized and ozone-treated carbon surfaces. Carbon

41(8): 1489–1500. Available at: https://doi.org/10.1016/S0008-6223(03)00053-8

Chopparapu R., Sambattula K. R., Edara D. K., Dasari R., Sycam V., Srivalli G. and Chennaiah M. B. (2020) A review article on water purification techniques by using fiber composites and biodegradable polymers. [Conference Proceedings] 040007. Available at: https://doi.org/10.1063/5.0004069

Choque-Quispe D., Froehner S., Ligarda-Samanez C. A., Ramos-Pacheco B. S., Peralta-Guevara D. E., Palomino-Rincón H., Choque-Quispe Y., Solano-Reynoso A. M., Barboza-Palomino G. I., Taipe-Pardo F. and Zamalloa-Puma L. M. (2021) Insights from water quality of high Andean springs for human consumption in Peru. Water 13(19): 2650. Available at: https://doi.org/10.3390/w13192650

Dao T.M. and Le Luu T. (2020) Synthesis of activated carbon from macadamia nutshells activated by H_2SO_4 and K_2CO_3 for methylene blue removal in water. Bioresource Technology Reports 12: 100583. Available at: https://doi.org/10.1016/j.biteb.2020.100583

Doğan M., Sabaz P., Bicil Z., Koçer Kizilduman B. and Turhan Y. (2020) Activated carbon synthesis from tangerine peel and its use in hydrogen storage. Journal of the Energy Institute 93(6): 2176–2185. Available at: https://doi.org/10.1016/j.joei.2020.05.011

De Medina-Salas L., Castillo-González E., Giraldi-Díaz M.R. and Blanco-Pérez B. (2022) Reaction kinetics in the vermicomposting process of peach waste. Life 12: 1290. Available at: https://doi.org/10.3390/life12091290

Dubey A. (2022) A study on effects of hard water on human health. Research Ambition: An International Multidisciplinary e-Journal 6(IV): 15–16. Available at: https://doi.org/10.53724/ambition/v6n4.06

Duranoğlu D., Trochimczuk A.W. and Beker Ü. (2010) A comparison study of peach stone and acrylonitrile-divinylbenzene copolymer-based activated carbons as chromium (VI) sorbents. Chemical Engineering Journal 165(1): 56–63. Available at: https://doi.org/10.1016/j.cej.2010.08.054

Fan M., Marshall W., Daugaard D. and Brown R.C. (2004) Steam activation of chars produced from oat hulls and corn stover. Bioresource Technology 93(1): 103–107. Available at: https://doi.org/10.1016/j.biortech.2003.08.016

Farah N. and Torell G.L. (2019) Defensive investment in municipal water hardness reduction. Water Resources Research 55(6): 4886–4900. Available at: https://doi.org/10.1029/2018WR024422

Figueiredo J.L., Pereira M.F.R., Freitas M.M.A. and Órfão J.J.M. (1999) Modification of the surface chemistry of activated carbons. Carbon 37(9): 1379–1389. Available at: https://doi.org/10.1016/S0008-6223(98)00333-9

Filippín A.J., Luna N.S., Pozzi M.T. and Pérez J.D. (2017) Obtención y caracterización de carbón activado a partir de residuos olivícolas y oleícolas por activación física [Obtaining and characterization of activated carbon from olive and olive residues by physical activation]. Avances en Ciencias e Ingeniería 8(3): 59–71. Available at: https://dialnet.unirioja.es/servlet/articulo?codigo=6308813&info=resumen&idioma=ENG (accessed 13 September 2024) (in Spanish).

Fortunato A.B., Bimbi Júnior F.E., Moreira J.M., et al. (2022) Buriti biomass as catalysts based on activated carbon/Fe3O4 for ciprofloxacin removal by heterogeneous photo-Fenton process. Journal of Water Process Engineering 50: 103263. Available at: https://doi.org/10.1016/j.jwpe.2022.103263

Gimba C.E., Ocholi O., Egwaikhide P.A., Muyiwa T. and Akporhonor E.E. (2009) New raw material for activated carbon: I. Methylene blue adsorption on activated carbon prepared from Khaya senegalensis fruits. Ciencia e Investigación Agraria 36(1). Available at: https://doi.org/10.4067/S0718-16202009000100010

Girgis B.S., Yunis S.S. and Soliman A.M. (2002) Characteristics of activated carbon from peanut hulls in relation to conditions of preparation. Materials Letters 57(1): 164–172. Available at: https://doi.org/10.1016/S0167-577X(02)00724-3

Gregg S.J., Sing K.S.W. and Salzberg H.W. (1967) Adsorption surface area and porosity. Journal of The Electrochemical Society 114(11): 279Ca. Available at: https://doi.org/10.1149/1.2426447

Guo J. and Lua A.C. (1999) Textural and chemical characterisations of activated carbon prepared from oil-palm stone with H2SO4 and KOH impregnation. Microporous and Mesoporous Materials 32(1–2): 111–117. Available at: https://doi.org/10.1016/S1387-1811(99)00096-7

Hernández-Vásquez A., Rojas-Roque C., Marques Sales D., Santero M., Bendezu-Quispe G., Barrientos-Gutiérrez T. and Miranda J.J. (2021) Inequalities in access to safe drinking water in Peruvian households according to city size: an analysis from 2008 to 2018. International Journal for Equity in Health 20(1): 133. Available at: https://doi.org/10.1186/s12939-021-01466-7

Iwanow M., Gärtner T., Sieber V. and König B. (2020) Activated carbon as catalyst support: precursors, preparation, modification and characterization. Beilstein Journal of Organic Chemistry 16: 1188–1202. Available at: https://doi.org/10.3762/bjoc.16.104

Javidi Alsadi K. and Esfandiari N. (2019) Synthesis of activated carbon from sugarcane bagasse and application for mercury adsorption. Pollution 5(3): 585–596.

Khalil K.M.S., Elhamdy W.A., Goda M.N. and Said A.E.-A.A. (2021) Biomass-derived P-containing activated carbon as a novel green catalyst/support for methanol conversion to dimethyl ether alternative fuel. Journal of Environmental Chemical Engineering 9(6): 106572. Available at: https://doi.org/10.1016/j.jece.2021.106572

Lam S.S., Liew R.K., Lim X.Y., Ani F.N. and Jusoh A. (2016) Fruit waste as feedstock for recovery by pyrolysis technique. International Biodeterioration and Biodegradation 113: 325–333. Available at: https://doi.org/10.1016/j.ibiod.2016.02.021

Li L., Quinlivan P.A. and Knappe D.R.U. (2002) Effects of activated carbon surface chemistry and pore structure on the adsorption of organic contaminants from aqueous solution. Carbon 40(12): 2085–2100. Available at: https://doi.org/10.1016/S0008-6223(02)00069-6

Lin, L., Yang, H., and Xu, X. (2022). Effects of Water Pollution on Human Health and Disease Heterogeneity: A Review., 10. Available at: https://doi.org/10.3389/fenvs.2022.880246

Lima S.S.A., Paiva S.C. de, Filho H.J.B. de L., Takaki G.M.C. and Messias A.S. (2020) Calcium and magnesium adsorption by activated carbon produced with alternative materials. Advances in Research: 1–6. Available at: https://doi.org/10.9734/air/2019/v20i630172

Meshram S., Thakur R.S., Jyoti G., Thakur C. and Soni A.B. (2022) Optimization of lead adsorption from lead-acid battery recycling unit wastewater using H_2SO_4 modified activated carbon. Journal of the Indian Chemical Society 99(6): 100469. Available at: https://doi.org/10.1016/j.jics.2022.100469

Ministerio de Comercio Exterior y Turismo del Perú (2007) [Ministry of Foreign Trade and Tourism of Peru]. Plan operativo del durazno: Región Lima Provincias (in Spanish).

Mo J., Yang Q., Zhang N., Zhang W., Zheng Y. and Zhang Z. (2018) A review on agro-industrial waste (AIW) derived adsorbents for water and wastewater treatment. Journal of Environmental Management 227: 395–405. Available at: https://doi.org/10.1016/j.jenvman.2018.08.069

Mohd S., Hooi L. and Marzuki M. (2015) Investigation of coconut shells activated carbon as the cost-effective absorbent in drinking water filter. Jurnal Teknologi 77: 2180–3722. Available at: www.jurnalteknologi.utm.my (accessed 20 September 2024).

Mojoudi N., Mirghaffari N., Soleimani M., Shariatmadari H., Belver C. and Bedia J. (2019) Phenol adsorption on high microporous activated carbons prepared from oily sludge: equilibrium, kinetic and thermodynamic studies. Scientific Reports 9(1): 19352. Available at: https://doi.org/10.1038/s41598-019-55794-4

Momeni M., Gharedaghi Z., Amin M.M., Poursafa P. and Mansourian M. (2010) Does water hardness have a preventive effect on cardiovascular disease? International Journal of Preventive Medicine 5(2). Available at: www.ijpm.ir (accessed 20 September 2024).

Mopoung S., Amornsakch P., Mopoung R. and Thianngam P. (2018) Potassium permanganate loaded activated carbon production from pineapple leaf at low pyrolysis temperature for water hardness removal. Asian Journal of Scientific Research 12(1): 126–136. Available at: https://doi.org/10.3923/ajsr.2019.126.136

Moreno-Castilla C. (2004) Adsorption of organic molecules from aqueous solutions on carbon materials. Carbon 42(1): 83–94. Available at: https://doi.org/10.1016/j.carbon.2003.09.022

Morris, R., Walker, M., Lennon, L., Shaper, A., and Whincup, P. (2008). Hard drinking water does not protect against cardiovascular disease: new evidence from the British Regional Heart Study. European Journal of Preventive Cardiology, 15, 185-189. Available at: https://doi.org/10.1097/HJR.0b013e3282f15fce

Mulwa F., Li Z. and Fangninou F.F. (2021) Water scarcity in Kenya: current status, challenges and future solutions. OALib 8(1): 1–15. Available at: https://doi.org/10.4236/oalib.1107096

Neolaka Y.A.B., Riwu A.A.P., Aigbe U.O., et al. (2023) Potential of activated carbon from various sources as a low-cost adsorbent to remove heavy metals and synthetic dyes. Results in Chemistry 5: 100711. Available at: https://doi.org/10.1016/j.rechem.2022.100711

Newcombe G., Hayes R. and Drikas M. (1993) Granular activated carbon: importance of surface properties in the adsorption of naturally occurring organics. Colloids and Surfaces A: Physicochemical and Engineering Aspects 78: 65–71. Available at: https://doi.org/10.1016/0927-7757(93)80311-2

Nyangi M. (2023) Simultaneous removal of chloride and hardness from groundwater by cassava peel biosorption: optimization and sorption studies. Remediation Journal. Available at: https://doi.org/10.1002/rem.21770

Otowa T., Tanibata R. and Itoh M. (1993) Production and adsorption characteristics of MAXSORB: high-surface-area active carbon. Gas Separation and Purification 7(4): 241–245. Available at: https://doi.org/10.1016/0950-4214(93)80024-Q

Peña K.J., Giraldo L. and Moreno J.C. (2012) Preparación de carbón activado a partir de cáscara de naranja por activación química. Caracterización física y química [Preparation of activated carbon from orange peel by chemical activation. Physical and chemical characterization]. Revista Colombiana de Química 41(2). Available at: http://www.scielo.org.co/pdf/rcq/v41n2/v41n2a10.pdf (accessed 2 October 2024) (in Spanish).

Pérez-López E. (2016) Control de calidad en aguas para consumo humano en la región occidental de Costa Rica [Quality control of water for human consumption in western Costa Rica]. Revista Tecnología en Marcha 29(3): 3. Available at: https://doi.org/10.18845/tm.v29i3.2884 (in Spanish).

Ramos Olmos R., Sepúlveda Marqués R. and Villalobos Moreto F. (2003) El agua en el medio ambiente: muestreo y análisis. Universidad Autónoma de Baja California, Plaza y Valdés [Water in the environment: sampling and analysis. Autonomous University of Baja California, Plaza y Valdés]. Avalaible at: https://biblioteca.ecosur.mx/cgi-bin/koha/opac-detail.pl?biblionumber=000045091 (accessed 05 October 2024) (in Spanish).

Reyna L. and Chuquilín C. (2006) Obtención de carbón activado y aceite esencial a partir del durazno (Blanquillo) [Obtaining activated carbon and essential oil from peach (Blanquillo)]. Revista Peruana de Química e Ingeniería Química 9(2): 38–43. Available at: https://revistasinvestigacion.unmsm.edu.pe/index.php/quim/article/view/4250 (accessed 2 July 2024) (in Spanish).

Rolence C., Machunda R. and Njau K. (2014) Water hardness removal by coconut shell activated carbon. International Journal of

Science, Technology and Society 2: 97. Available at: https://doi.org/10.11648/j.ijsts.20140205.11

Rostami E., Esfandiari N., Honarvar B., et al. (2022) Kinetic and thermodynamic parameters of cadmium ion removal by using the orange wood-synthesized activated carbon nanoparticles modified with cysteine. Pollution 8(4): 1216–1232.

Rostami E., Esfandiari N., Honarvar B. et al. (2023) Comparison of activated carbon from bitter orange and Amygdalus scoparia Spach and surface modification. Biomass Conversion and Biorefinery 13: 17255–17269. Available at: https://doi.org/10.1007/s13399-022-03024-9

Rostamian R., Heidarpour M., Mousavi S.F. and Afyuni M. (2014) Removal of calcium and magnesium by activated carbons produced from agricultural wastes. Advances in Environmental Biology: 202–209. Available at: https://go.gale.com/ps/i.do?p=AONE&sw=w&issn=19950756&v=2.1&it=r&id=GALE%7CA385260346&sid=googleScholar&linkaccess=fulltext (accessed 8 July 2024).

Salehi M. (2022) Global water shortage and potable water safety; today's concern and tomorrow's crisis. Environment International 158: 106936. Available at: https://doi.org/10.1016/j.envint.2021.106936

Sengupta P. (2013) Potential health impacts of hard water. International Journal of Preventive Medicine 4: 866–875. Available at: https://api.semanticscholar.org/CorpusID:5392521 (accessed 6 July 2024).

Shin S., Jang J., Yoon S.-H. and Mochida I. (1997) A study on the effect of heat treatment on functional groups of pitch-based activated carbon fiber using FTIR. Carbon 35(12): 1739–1743. Available at: https://doi.org/10.1016/S0008-6223(97)00132-2

Snyder E.E., Buoscio B.W. and Falke J.J. (1990) Calcium(II) site specificity: effect of size and charge on metal ion binding to an EF-hand-like site. Biochemistry 29(16): 3937–3943. Available at: https://doi.org/10.1021/bi00468a021

SUNASS (Superintendencia Nacional de Servicios de Saneamiento) (2004) Análisis de la calidad del agua potable en las empresas prestadoras del Perú: 1995-2003 [Analysis of drinking water quality in Peruvian utilities: 1995-2003]. Available at: https://www.sunass.gob.pe/wp-content/uploads/2020/09/Jica-2003.pdf (accessed 8 May 2024) (in Spanish).

Takmil F., Esmaeili H., Mousavi S.M. and Hashemi S.A. (2020) Nano-magnetically modified activated carbon prepared by oak shell for treatment of wastewater containing fluoride ion. Advanced Powder Technology 31(8): 3236–3245. Available at: https://doi.org/10.1016/j.apt.2020.06.015

Tarrass F. and Benjelloun M. (2012) The effects of water shortages on health and human development. Perspectives in Public Health 132(5): 240–244. Available at: https://doi.org/10.1177/1757913910391040

Tomar Y. (2018) Removal of chloride, hardness and TDS from water using different adsorbents. International Journal for Research in Applied Science and Engineering Technology 6: 5111–5117. Available at: https://doi.org/10.22214/ijraset.2018.4834

Tsoncheva T., Mileva A., Tsyntsarski B., Paneva D., Spassova I., Kovacheva D., Velinov N., Karashanova D., Georgieva B. and Petrov N. (2018) Activated carbon from Bulgarian peach stones as a support of catalysts for methanol decomposition. Biomass and Bioenergy 109: 135–146. Available at: https://doi.org/10.1016/j.biombioe.2017.12.022

Ukanwa K., Patchigolla K., Sakrabani R., Anthony E. and Mandavgane S. (2019) A review of chemicals to produce activated carbon from agricultural waste biomass. Sustainability. Available at: https://doi.org/10.3390/su11226204

Uysal T., Duman G., Onal Y., Yasa I. and Yanik J. (2014) Production of activated carbon and fungicidal oil from peach stone by two-stage process. Journal of Analytical and Applied Pyrolysis 108: 47–55. Available at: https://doi.org/10.1016/j.jaap.2014.05.017

Van Vliet M.T.H., Jones E.R., Flörke M., Franssen W.H.P., Hanasaki N., Wada Y. and Yearsley J.R. (2021) Global water scarcity including surface water quality and expansions of clean water technologies. Environmental Research Letters 16(2): 024020. Available at: https://doi.org/10.1088/1748-9326/abbfc3

Vanegas G. (2021) Preparación y caracterización de carbón activado obtenido a partir de residuos textiles de mezclilla [Preparation and characterization of activated carbon obtained from denim textile waste]. Universidad Nacional de Colombia. Available at: https://repositorio.unal.edu.co/handle/unal/81024 (accessed 8 May 2024) (in Spanish).

Varada K. (2018) Adsorption studies on water hardness removal by using Moringa oleifera seed pod husk activated carbon as an adsorbent.

Wang X., Guo Z., Hu Z. and Zhang J. (2020) Recent advances in biochar application for water and wastewater treatment: a review. PeerJ 8: e9164. Available at: https://doi.org/10.7717/peerj.9164

Xing X., Zhang Y., Zhou G., Zhang Y., Yue J., Wang X., Yang Z., Chen J., Wang Q. and Zhang J. (2023) Mechanisms of polystyrene nanoplastics adsorption onto activated carbon modified by $ZnCl_2$. Science of The Total Environment 876: 162763. Available at: https://doi.org/10.1016/j.scitotenv.2023.162763

Zhao H., Zhong H., Jiang Y., Li H., Tang P., Li D. and Feng Y. (2022) Porous $ZnCl_2$-activated carbon from shaddock peel: methylene blue adsorption behavior. Materials 15(3): 895. Available at: https://doi.org/10.3390/ma15030895

This article is an Open Access article distributed under the terms and conditions of the Creative Commons Attribution 4.0 (CC BY 4.0) License (http://creativecommons.org/licenses/by/4.0/).